Ultrafast pump-and-probe spectroscopy in CdSe: Hot-carrier and exciton dynamics

Fumio Sasaki, Tomobumi Mishina, and Yasuaki Masumoto
Institute of Physics, University of Tsukuba, Tsukuba, Ibaraki 305, Japan
(Received 30 December 1991)

An extensive study by means of femtosecond pump-and-probe spectroscopy has clarified the ultrafast dynamics of photogenerated carriers in a CdSe thin film. Under band-to-band excitation, a nonthermalized hot-carrier distribution was observed immediately upon excitation. This distribution was observed in a 200-meV broad energy range extending from the pump energy to its low-energy side. Its low-energy tail indicates that carrier-LO-phonon scattering competes with carrier-carrier scattering in the thermalization process. From the ratio of nonthermalized to the total carriers, the thermalization time was estimated to be 20–40 fs. In the wake of thermalization, cooling of photogenerated carriers was observed. With an increase of the excitation density up to 10^{19} cm^{-3}, the carrier cooling rate was slower. The cooling rate observed at 4.2 K was comparable to that at room temperature. The observed cooling rate was slower than that predicted by a theoretical calculation which took into account screening of the carrier-phonon interaction. This is ascribed to hot-phonon effects of LO phonons and TO phonons. Under resonant excitation of the A exciton, a 42-meV energy broadening of the B-exciton structure was observed. This broadening is caused by collisions between the A exciton and the B exciton. This is an example of the scattering process between different kinds of excitons. Analysis indicates that the A-exciton–B-exciton scattering time is 31 fs. This time is well explained by a simple theory based on the rigid-sphere scattering model. The broadening decreases with a time constant on the order of hundreds of picoseconds. This time constant is well explained by the lifetime of the excitons. Under resonant excitation of the B exciton, a fast recovery of the bleaching was observed at the B exciton. The recovery time of 0.9 ps is explained as the transformation time of B excitons into A excitons by LO-phonon emission. The obtained time constant agrees with the calculated scattering time based on the Fröhlich interaction within an order of magnitude.

I. INTRODUCTION

With recent advances in ultrafast laser spectroscopy, we can observe dynamical processes of carriers in semiconductors. The hot-carrier effect in semiconductors is one of the most important subjects in these studies. From a fundamental point of view, we can directly observe the dynamical carrier distribution and study the relaxation processes in semiconductors. Hot-carrier phenomena are determined primarily by band structures and carrier-phonon scattering processes. Therefore, studies of hot-carrier phenomena provide important information about carrier-phonon interactions. On the other hand, hot-carrier physics regulates the behavior of ultrafast, ultrasmall semiconductor devices operating at high electric fields. Therefore, a study of hot-carrier effects is important in understanding such devices.[1]

Up to now, hot-carrier systems have been extensively studied by means of transport experiments and luminescence spectroscopy around the fundamental gap of semiconductors. With advances in ultrafast laser spectroscopy, time-resolved absorption experiments have been adopted to study this subject. These studies have clarified the dynamics of hot carriers as follows.

Initially, photoexcited carriers are distributed at the energy of the pump pulse. Transient spectral hole burning has been experimentally observed in three-dimensional (3D),[2,3] two-dimensional,[4,5] and zero-dimensional[6] systems. The transient spectral hole diminishes in several tens or hundreds of femtoseconds depending on the excitation photon energy and density. After the transient hole diminishes, only bleaching below the pump photon energy is observed. The bleaching profile shows the carrier distribution. Generally, photoexcited carriers are thermalized by carrier-carrier scattering. The scattering time is found to be on the order of a few or a few tens of femtoseconds by means of femtosecond photon echo in GaAs.[7] In the studies of the thermalization process, experiments have dealt with the carrier-carrier scattering process. However, high-energy carriers can emit optical phonons. In this case, carrier-carrier scattering competes with optical-phonon emission. Therefore, the study of high-energy carriers enables us to observe the competition between the two processes.

Recently, one of the carrier scattering processes, an intervalley scattering process, has been extensively studied.[8] If the conduction or the valence bands have a valley minimum other than the Γ point and photoexcited carriers have enough excess energy, they can scatter to that valley. Through recent studies of GaAs and $Al_xGa_{1-x}As$ systems, the Γ-X or the Γ-L scattering is observed and it is found that the scattering time is several tens of femtoseconds. The study of the multivalley scattering mechanism is very interesting and important in itself, but such a scattering mechanism makes it difficult to study high-energy carrier distributions in GaAs systems. Unlike GaAs systems, CdSe does not suffer from intervalley scattering and, therefore, is ideal for the study

of high-energy carrier distributions.

In the succeeding time region, photoexcited carriers emit phonons and lose their energy. The cooling rate depends strongly on the carrier-phonon scattering rate. There are three types of carrier-phonon interaction mechanisms: the Fröhlich interaction, the piezoelectric interaction, and the deformation-potential interaction. If a photoexcited carrier has excess energy larger than the LO-phonon energy, carrier-LO-phonon scattering is the fastest of the three processes. If not, the other two scattering processes are the main channels of energy transfer from the carrier system to the lattice.[9,10] In order to clarify the carrier cooling mechanism, we must consider the other effects that modify the carrier-phonon interaction. One is a screening of the carrier-LO-phonon interaction by highly excited carriers.[11–13] The other is a nonequilibrium phonon distribution effect, called a hot-phonon effect.[1,12–15] Both effects make the carrier cooling very slow. In recent studies, the latter effect is found to be the dominant mechanism of slow carrier cooling in the GaAs system.[15] The fastest carrier-phonon interaction, the carrier-polar-optical-phonon scattering takes place in the region of tens or hundreds of femtoseconds. Therefore, femtosecond spectroscopy is a powerful tool to study the hot-phonon effect.

From the above-mentioned considerations, we have studied hot-carrier effects in a thin CdSe film by femtosecond pump-and-probe spectroscopy under high-energy excitation. Since CdSe has no multivalley in the conduction or valence band under 4-eV photoexcitation, we consider only scattering mechanisms in the Γ valley. Therefore, we can study a dynamical carrier distribution confined to the Γ valley at high-energy excitation. As a result, a nonequilibrium distribution was observed immediately upon excitation. The nonthermalized distribution extended from the pump energy to its low-energy side. This feature shows the competition between carrier-carrier scattering and carrier-LO-phonon scattering.

One of the other interests in femtosecond spectroscopy is to clarify dynamics or optical nonlinearities of excitons in semiconductors.[16] Studies of exciton-exciton scattering processes and exciton-phonon scattering processes reveal the origin of the large optical nonlinearity of excitons. Therefore, these studies are necessary for the design and fabrication of optoelectronic devices. In CdSe, A-exciton and B-exciton peaks are observed near the fundamental absorption edge. The energy splitting between the A exciton and the B exciton is comparable to the LO-phonon energy. This situation is suitable for the study of collisions between A excitons and B excitons or exciton-LO-phonon scattering.

In Sec. II, the experimental condition of the pump-and-probe experiments is described. In Sec. III, discussions about hot-carrier systems under band-to-band excitation are given. In Sec. IV, we discuss the dynamics of excitons under resonant excitation.

II. EXPERIMENTS

In this study, two short-pulse laser sources were utilized. The first laser source consists of a cw mode-locked Nd^{3+}:YAG (YAG denotes yttrium aluminum garnet) laser, the first-stage fiber compressor, a second-harmonic generator, a synchronously pumped cavity-dumped dye laser, the second-stage fiber compressor, and a dye amplifier pumped by a Q-switched Nd^{3+}:YAG laser. In this case, the pump-phonon energy was 2.12 eV and pulse energy was about 400 μJ with a 260-fs pulse width. The laser pulses were split into two beams. One beam was focused on a water cell and generated white continuum-femtosecond pulses. The white-light beam was used as a probe beam and the desired spectral range was selected with color filters. The pump beam was sent through an optical delay. The excitation and probe beam power were varied by using rotational neutral-density filters that produce no change in the time delay or in the dispersion. The diameters of the spot and overlap of the two beams were checked with a microscope.

The second laser source was based on a colliding-pulse mode-locked dye laser and a multipass amplifier pumped by a Cu-vapor laser. This laser system is operational in the Optical Sciences Center of the University of Arizona and was used for some of the experiment reported in this paper. The amplified beam was focused on an ethylene-glycol jet and generated a white-light continuum. Part of the white light was used as a weak probe beam. The remaining part was sent through an interferential filter with a band width of about 10 nm. This beam was amplified using another multipass amplifier and used as the pump. With this system, we can tune the pump-photon energy to the A-exciton and B-exciton resonances. The pump pulse width was between 110 and 130 fs, depending on the photon energy. To reduce the scattered pump light, especially in the case of resonant pump experiments, the pump-and-probe beams were polarized orthogonally and an analyzer in the detection system selected only the probe light.

In femtosecond experiments, one difficulty comes from dispersion compensation. If we want to observe a wide-range spectrum, we must suppress the dispersion of the optics as far as possible. The temporal dispersion of the probe in these systems was less than 10 fs/nm. Taking into account the second-order term in the dispersion, a least-squares fit of the experimental dispersion was done. The agreement between the experimental results and the fit was very good, and the maximum deviation of the data from the fitting curve was smaller than 10 fs. Based on this fit, the time delays of the probe spectra were given a wavelength-dependent correction. In this way, time-resolved spectra were obtained in a wide energy range.

The sample was a 0.65-μm-thick CdSe thin film grown on a mica substrate by means of hot-wall epitaxy. The crystal c axis was perpendicular to the mica substrate. A mica substrate is suitable for the absorption experiment because it is transparent to visible light. Moreover, mica is a layered compound and its interlayer interaction comes from van der Waals force. Therefore, the strain between a mica substrate and a CdSe crystal is considered to be much smaller than other systems. Typical transmissivity at the pump photon energy was about 5% in this sample.

Four experiments were conducted: (1) pump at 2.12

eV with a pulse width of 260 fs at 4.2 K, (2) pump at 2.12 eV with a pulse width of 260 fs at room temperature, (3) pump at 1.86 eV with a pulse width of 110 fs at 10 K, and (4) pump at 1.82 eV with a pulse width of 130 fs at 10 K. Experiments (1) and (2) correspond to band-to-band excitation. Experiments (3) and (4) correspond to resonant excitation of the B exciton and A exciton, respectively. The data acquisition was done using an optical multichannel analyzer and a 25-cm spectrometer with low dispersive gratings (300 or 600 groves/mm) to obtain a wide-energy-range spectrum.

III. EXPERIMENTAL RESULTS UNDER BAND-TO-BAND EXCITATION AND DISCUSSIONS

A. Nonequilibrium distribution of photoexcited carriers

Under band-to-band excitation, a large number of free carriers is generated with kinetic energy greater than the optical-phonon energy by an intense optical pulse. The kinetic energy per carrier was on the order of 100 meV, which depends on the difference between the band gap and the excitation photon energy. The estimated carrier density was on the order of 10^{19} cm^{-3}.

Figures 1 and 2 show time-resolved absorption spectra under experimental conditions (1) and (2). Condition (1) corresponds to the 2.12-eV excitation at 4.2 K and condition (2) to the same excitation at room temperature. The excitation densities were 900 and 600 μJ cm^{-2}, respectively. The absorption spectra denoted "NO PUMP" were obtained from probe transmission in the absence of the pump pulses. Structures of the A exciton and the B exciton are clearly observed in Fig. 1. In Fig. 2, the A-exciton structure is observed as a kink around 1.76 eV. The spectrum at 0 ps shows a broad spectral dip around 2.0 eV in Fig. 1. There seems to be a broader spectral dip around 1.9 eV in Fig. 2. These features are due to a non-

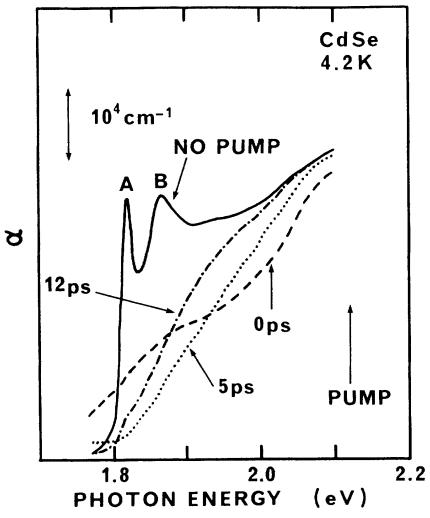

FIG. 1. Time-resolved absorption spectra of CdSe observed under 2.12-eV excitation at 4.2 K. The solid line denoted by "NO PUMP" shows the spectrum without the pump. Pump-and-probe spectra at 0-, 5-, and 12-ps time delays are shown.

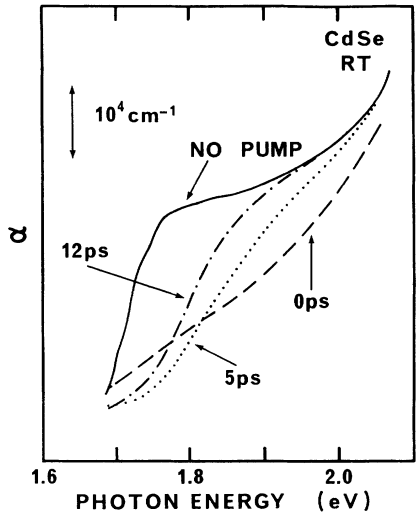

FIG. 2. Time-resolved absorption spectra of CdSe observed under 2.12-eV excitation at room temperature. The solid line denoted by "NO PUMP" shows the spectrum without the pump. Pump-and-probe spectra at 0-, 5-, and 12-ps time delays are shown.

thermalized distribution of hot carriers. In order to see the carrier distribution clearly, we plotted the time-resolved absorption spectra in the form of $-\Delta\alpha/\alpha$, where α and $\Delta\alpha$ denote the absorption coefficient and the change of α induced by the optical pumping, respectively. Figures 3 and 4 show these spectra under experimental conditions (1) and (2), respectively.

The relation between $-\Delta\alpha/\alpha$ and an electron (hole) distribution function $f_e(E_e)$ [$f_h(E_h)$] is expressed by[17]

$$-\Delta\alpha/\alpha = f_e(E_e) + f_h(E_h) \ . \tag{3.1}$$

Here, E_e and E_h denote the kinetic energy of electrons and holes, respectively. The kinetic energies of an electron and a hole are represented by

$$E_i = (\mu/m_i)(E - E_g) \quad (i = e,h) \ , \tag{3.2}$$

where μ, m_i, E, and E_g denote the reduced mass of an electron and a hole, an effective mass, the probe photon energy, and the band gap, respectively. In this analysis, one may take into account the anisotropy in the A-hole band. This simple expression (3.1) is then modified.[18] In order to estimate the anisotropy effect in the absorption spectrum, a calculation with and without the anisotropy was done. The calculation method is outlined in the Appendix. Figure 13 in the Appendix shows that the anisotropy effect is small. Therefore, we have neglected it for simplicity.

Further, we approximately replaced the right-hand side of Eq. (3.1) at the high-energy tail by the larger term. Because both $f_e(E_e)$ and $f_h(E_h)$ are the exponentially decaying functions at the high-energy tail, the smaller term is considered to be negligible compared with the larger term. Then, analysis procedures become simple as follows.[19]

We analyzed the $-\Delta\alpha/\alpha$ spectra by fitting the single

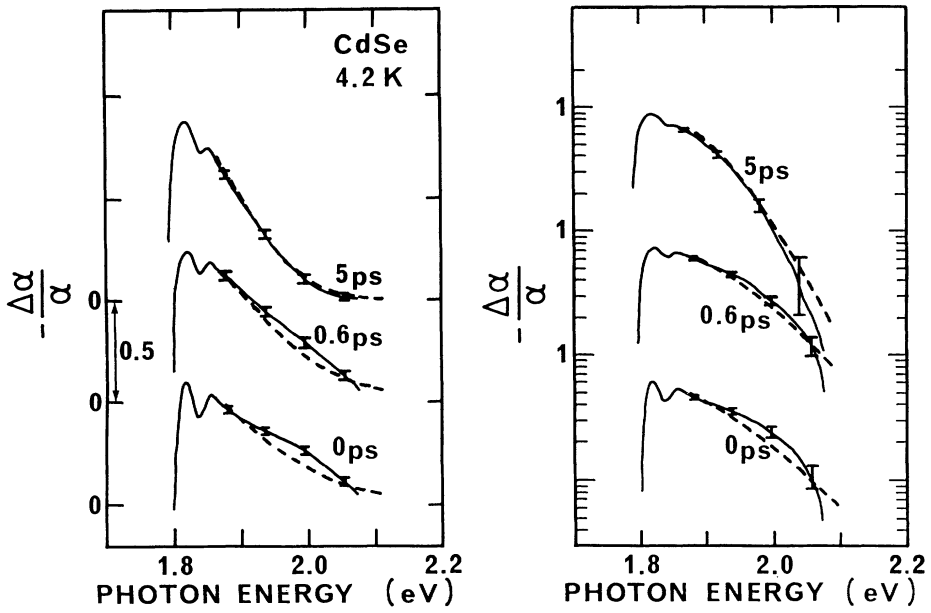

FIG. 3. The change in the absorption coefficient divided by the unperturbed absorption coefficient $-\Delta\alpha/\alpha$ observed under 2.12-eV excitation at 4.2 K. The left-hand part shows $-\Delta\alpha/\alpha$ in the linear scale, and the right-hand part shows $-\Delta\alpha/\alpha$ in the logarithmic scale. The effective temperature of hot carriers, T_c, is estimated from the fitting shown by dashed lines. Values of T_c for spectra at 0, 0.6, and 5 ps are 970, 850, and 540 K, respectively.

Fermi distribution function

$$f_c(E)=1/\{\exp[(E-E_F)/k_BT_c]+1\}\ ,$$

where E_F, T_c, and k_B denote the chemical potential, the effective temperature of hot carriers, and the Boltzmann constant, respectively. Almost all the spectra can be well fitted by a single Fermi distribution function except the spectra around the time origin. The spectra at 5 ps are well fitted by a single Fermi distribution function as shown in Figs. 3 and 4. However, the spectra observed at 0 ps cannot be fitted. Moreover, the spectrum shows a convex part around 2.0 eV in Fig. 3. In Fig. 4, the spectrum observed around 1.9 eV is not concave upward.

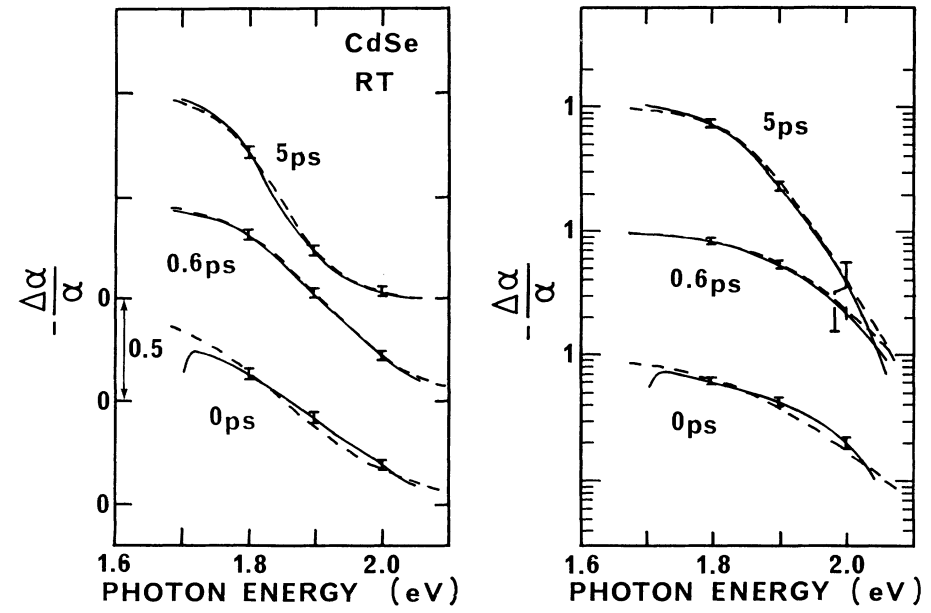

FIG. 4. The change in the absorption coefficient divided by the unperturbed absorption coefficient $-\Delta\alpha/\alpha$ observed under 2.12-eV excitation at room temperature. The left-hand part shows $-\Delta\alpha/\alpha$ in the linear scale and the right-hand part shows $-\Delta\alpha/\alpha$ in the logarithmic scale. The effective temperature of the hot carriers, T_c, is estimated from the fitting shown by dashed lines. Values of T_c for spectra at 0, 0.6, and 5 ps are 1100, 860, and 560 K, respectively.

The Fermi distribution function is concave upward below its value of 0.5. Therefore, the spectra observed around 2.0 eV in Fig. 3 and 1.9 eV in Fig. 4 indicate a nonthermalized distribution of hot carriers.

This nonequilibrium distribution of hot carriers was thermalized before the end of the pump pulse by carrier-carrier scattering. So far, the thermalization time has been estimated in 3D GaAs by means of femtosecond pump-and-probe spectroscopy.[2] In that experiment, carriers had small excess energy and were not able to emit an LO phonon. However in our experiment, carriers had enough excess energy to scatter and emit LO phonons. Therefore, the nonthermalized distribution observed in this experiment spread over a 200-meV-broad energy range. The low-energy tail of the nonthermalized distribution indicates that the carrier-LO-phonon scattering process competes with the carrier-carrier scattering process.

The thermalization time could not be observed in the time trace because of the limited time resolution, but we estimated the thermalization time from the spectra at 0 ps. A simple rate equation is written by

$$dn/dt = g(t) - n/\tau_d \ , \tag{3.3}$$

where n, $g(t)$, and τ_d denote the carrier density, the generation rate of the photoexcited carriers, and the decay rate, respectively. We can neglect the decay term because of the fairly long lifetime of carriers. We separate the nonthermalized carrier density n^n from the equilibrium carrier density n^e. Then, Eq. (3.3) becomes

$$dn^n/dt = g(t) - n^n/\tau \ , \quad dn^e/dt = n^n/\tau \ , \tag{3.4}$$

where τ denotes the thermalization time constant. If the generation rate is constant within the experimental time resolution δt, the nonthermalized carrier density at time

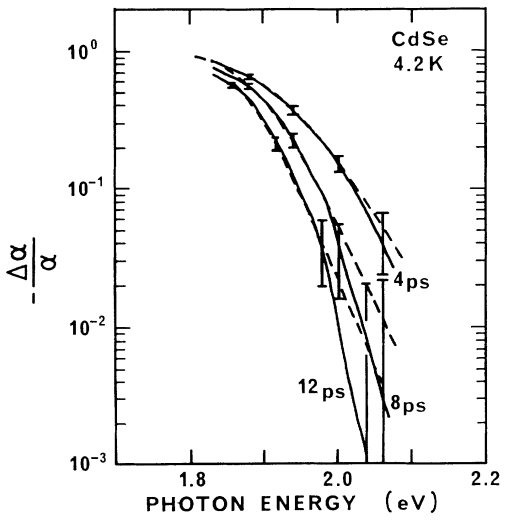

FIG. 5. The change in the absorption coefficient divided by the unperturbed absorption coefficient $-\Delta\alpha/\alpha$ observed under 2.12-eV excitation at 4.2 K (solid lines). The vertical scale is logarithmic. The fitted Fermi distribution functions are shown by dashed lines. Values of the estimated temperature for spectra at 4, 8, and 12 ps are 580, 440, and 390 K, respectively.

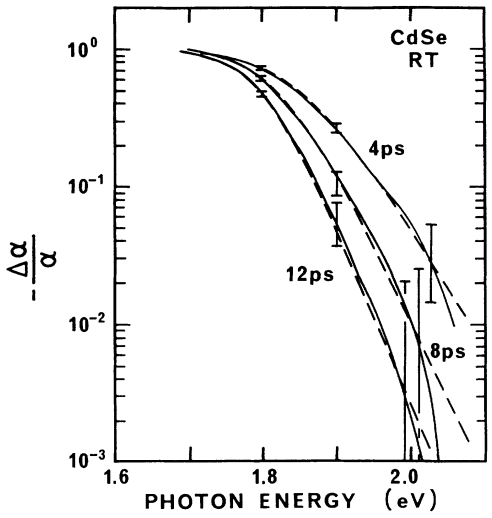

FIG. 6. The change in the absorption coefficient divided by the unperturbed absorption coefficient $-\Delta\alpha/\alpha$ observed under 2.12-eV excitation at room temperature (solid lines). The vertical scale is logarithmic. The fitted Fermi distribution functions are shown by dashed lines. Values of the estimated temperature for spectra at 4, 8, and 12 ps are 590, 460, and 400 K, respectively.

δt is represented by

$$n^n(\delta t) = \int_{-\infty}^{\delta t} \frac{\delta n}{\delta t} \exp[(t' - \delta t)/\tau] dt' = \frac{\delta n}{\delta t}\tau \ . \tag{3.5}$$

Here, δn denotes the total carrier density generated within the time resolution. Equation (3.5) shows that the thermalization time τ is estimated to be $(n^n/\delta n)\delta t$.

From the experimental results shown in Figs. 3 and 4, the ratios of the nonthermalized distribution to the total one were obtained as 10% for the spectrum at 0 ps in 4.2

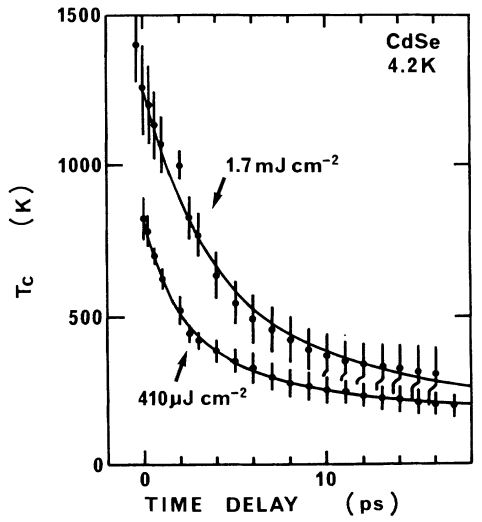

FIG. 7. Temporal change of the estimated temperature, T_c, observed at 4.2 K. Solid circles show experimentally estimated temperatures. Solid lines are the numerically fitted result. Upper and lower curves show the data obtained under 1.7-mJ cm^{-2} and 410-μJ cm^{-2} excitation, respectively.

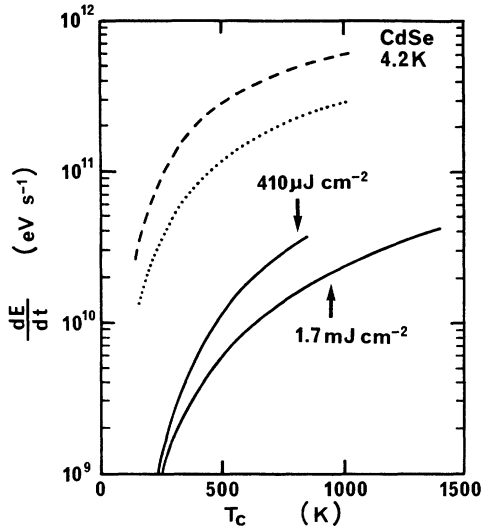

FIG. 8. Solid lines show the energy-loss rate of hot carriers observed at 410-μJ cm^{-2} and 1.7-mJ cm^{-2} excitation. Dashed and dotted lines show the calculated energy-loss rate at carrier densities of 1×10^{19} and 6×10^{19} cm^{-3}, respectively.

K and 5% at room temperature. Therefore, approximately 5–10% of the present time resolution of 400 fs roughly gives the thermalization time of 20–40 fs.

B. Cooling of hot carriers

Cooling of hot carriers was observed in the picosecond time regime. Figure 5 shows the data taken at 4.2 K and Fig. 6 shows the data taken at room temperature. In this time regime, the spectra are well described by a Fermi distribution as shown by the dashed line in Figs. 5 and 6. Therefore, cooling of the hot carriers is characterized by an effective temperature of the hot carriers. The fitted carrier temperatures at 4, 8, and 12 ps are 580, 440, and 390 K, respectively, in Fig. 5. In Fig. 6, those at 4, 8, and 12 ps are 590, 460, and 400 K, respectively. The fitted carrier temperature at 4.2 K is similar to that at room temperature. This fact indicates that the cooling rate observed at 4.2 K is comparable with that observed at room temperature, since the carrier temperature is much higher than the lattice temperature.

The temporal changes of T_c observed at different excitation densities are plotted in Fig. 7. The lower and upper curves show the results observed at the excitation density of 410 μJ cm^{-2} and 1.7 mJ cm^{-2}, respectively. The carrier densities estimated from the transmissivity of the pump pulse were 1×10^{19} and 6×10^{19} cm^{-3}, respectively. Solid circles are the fitted carrier temperature. Vertical bars are error bars of the fitting. In order to compare the observed carrier cooling rate with a calculated rate, we differentiated these curves by time. After fitting the experimental data by the solid lines shown in Fig. 7, we took the differential of the curves. The results are shown by solid lines in Fig. 8 as a function of T_c. This result shows that the carrier cooling rate slows with an increase of excitation density. The dashed and dotted curves show the calculated energy-loss rate based on screening of the carrier-phonon interaction.[12,13]

In this calculation, we took into account four carrier-phonon interactions: the carrier-LO-phonon scattering based on the Fröhlich interaction, the carrier-acoustic-phonon scattering based on the piezoelectric scattering, the carrier-TO-phonon scattering based on the optical deformation-potential scattering, and the carrier-acoustic-phonon scattering based on the deformation-potential scattering. The energy-loss-rate formula and parameters used in the calculations were those in Ref. 13.

As a result of the calculation, the dashed and dotted curves were obtained at carrier densities of 1×10^{19} and 6×10^{19} cm^{-3}, respectively. These densities are the values estimated from the experiment. The disagreement between the observed energy-loss rate and the calculated rate is probably due to the hot-phonon effect. At these high carrier densities, the screening of the Fröhlich interaction works more sensitively than that of the optical deformation-potential interaction, so that the energy-loss rate by LO-phonon emission is found to be comparable with that by TO-phonon emission. Therefore, the observed slow energy-loss rate is attributed to the hot-phonon effects of both LO and TO phonons.

IV. EXPERIMENTAL RESULTS UNDER RESONANT EXCITATION OF EXCITONS AND DISCUSSIONS

A. *A*-exciton resonant excitation

Figure 9 shows the change in the absorption spectra $-\Delta\alpha$ under resonant excitation of the A exciton. The bleaching has peaks at both the A-exciton and B-exciton resonances. Initially, induced absorption is observed around the A-exciton resonance. The induced absorption observed at the low-energy side of the A exciton diminishes with time. As this occurs, the induced absorption at the high-energy side of the B exciton grows. Such a

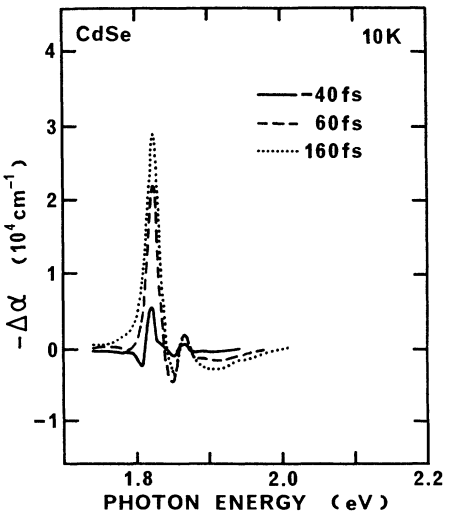

FIG. 9. Time-resolved absorption change $-\Delta\alpha$ observed under resonant excitation of the A exciton at 10 K around the time origin.

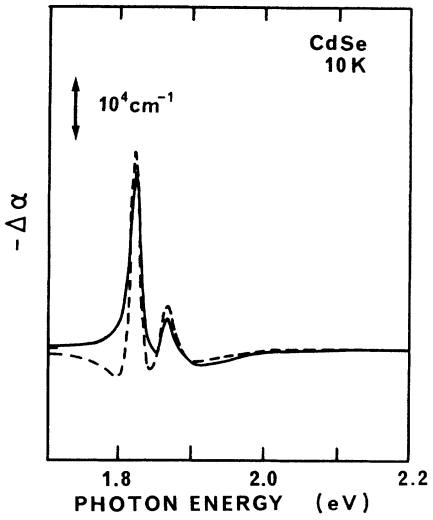

FIG. 10. Fitting of line broadening. The solid line shows an experimental spectrum observed under A-exciton resonant excitation at 560 fs. The dashed line shows a calculated spectrum based on the broadening of two Lorentzian functions.

spectral change is interpreted as a broadening of both the absorption lines. We ascribe this energy broadening of each absorption line to collisional broadening of excitons.

The collisional broadening of excitons in GaAs was previously observed in Figs. 1 and 2 of Ref. 4 by femtosecond pump-and-probe experiments. In that experiment, excitons collide with free carriers. In our experiment, A excitons were initially excited at 10 K, which is too low a temperature to ionize the exciton. Therefore, the energy broadening of the B-exciton resonance is caused by mutual collisions between A excitons and B excitons. This is an example of collisions among different kinds of excitons. Another example of collisions between different kinds of excitons was recently reported for magnetoexcitons in GaAs quantum wells.[20]

The broadening of the exciton line yields the scattering time of the excitons. The spectral shape of an absorption line caused by collisional broadening is represented by a Lorentzian function. In this case, the relation between the energy width (full width at half maximum) ΔE and the mean scattering time τ_s is expressed by $\Delta E \tau_s \sim 2\hbar$. From this relation, we can estimate the exciton-exciton scattering time. In order to obtain the energy broadening ΔE, we fitted the calculated spectrum to the experimental spectrum $-\Delta\alpha$, as shown in Fig. 10. In this fitting, we used two Lorentzian functions. The solid and dashed lines show the experimental spectrum observed at 560 fs and the fitted spectrum. The induced absorption observed at the high-energy side of the B exciton is well fitted.

Initially, broadening of the A exciton is observed below the A-exciton peak, as shown in Fig. 9. The broadening below the A exciton disappears as soon as the bleaching become large. The bleaching caused by phase-space filling is observed at the low-energy side of the A exciton and balances the effects of the broadening. However, the broadening observed above the A exciton remains and is not masked by the bleaching.

The fitting showed the energy broadening of the B exciton and the A exciton to be about 42 and 27 meV, respectively. Inserting these values into the equation $\Delta E \tau_s \sim 2\hbar$, we obtain a scattering time of 31 fs between the B excitons and the A excitons. We also obtain a mean scattering time of 49 fs between the A excitons and the A excitons.

The exciton-exciton scattering rate was experimentally determined using time-resolved degenerate four-wave mixing,[21] and was theoretically calculated by Manzke, Henneberger, and May.[22] However, these studies only dealt with collisions between the same excitons or between excitons and free carriers. It is difficult to model the collision processes between different kinds of excitons taking into account the many-particle problems. Therefore, we estimate the collision rate from a simple theory. Since excitons have no charge, we use a model of rigid-sphere scattering as the scattering mechanism of excitons. We assume that the photoexcited A excitons obey the Boltzmann distribution at the lattice temperature T_L. The B excitons generated by a probe pulse collide with the A excitons. In this case, the A exciton and B exciton mutual scattering rate $1/\tau_{A\text{-}B}$ is represented by

$$1/\tau_{A\text{-}B} = 2n_{\rm ex}(a_A + a_B)^2 (2\pi k_B T_L / M_{AB})^{1/2} , \quad (4.1)$$

where $n_{\rm ex}$, M_{AB}, a_A, and a_B denote the A-exciton density, the reduced mass between the A exciton ($0.93m_0$) and the B exciton ($1.03m_0$), the Bohr radius of the A exciton (5.3 nm), and that of the B exciton (4.9 nm), respectively. Here, m_0 denotes the bare electron mass. In the experiments, the values of $n_{\rm ex}$ and T_L were 3×10^{18} cm^{-3} and 10 K, respectively. The calculated scattering time is 36 fs. The agreement between the observed 31 fs and estimated 36 fs is very good. Utilizing this model, the broadening of the B-exciton resonance is well explained by the A-exciton–B-exciton collisional broadening.

The energy broadening of both excitons is found to increase consistently with the excitation density. This fact also supports this model. In this simple model, however, the A-exciton–A-exciton collision time $\tau_{A\text{-}A}$ is 34 fs, which is comparable with the A-exciton–B-exciton collision time. The difference between $\tau_{A\text{-}A}$ and $\tau_{A\text{-}B}$ obtained from the experiment cannot be explained by this model. This may be due to the Pauli exclusion between the A exciton and another A exciton.

B. B-exciton resonant excitation

Figure 11 shows the results of resonant excitation of the B exciton. The left-hand part of this figure shows the spectra around the time origin and the right-hand part shows the spectra in the picosecond regime. Initially, the bleaching of both the A exciton and the B exciton increases at the same time. However, the bleaching at the B exciton decreases more rapidly than that at the A exciton, as shown in the right-hand part of Fig. 11. The time dependence of the bleaching at the B exciton is plotted in Fig. 12. The solid line shows the experimental result and the dashed line shows the fit to a double-exponentially decaying function. From the fitting, the time constants of

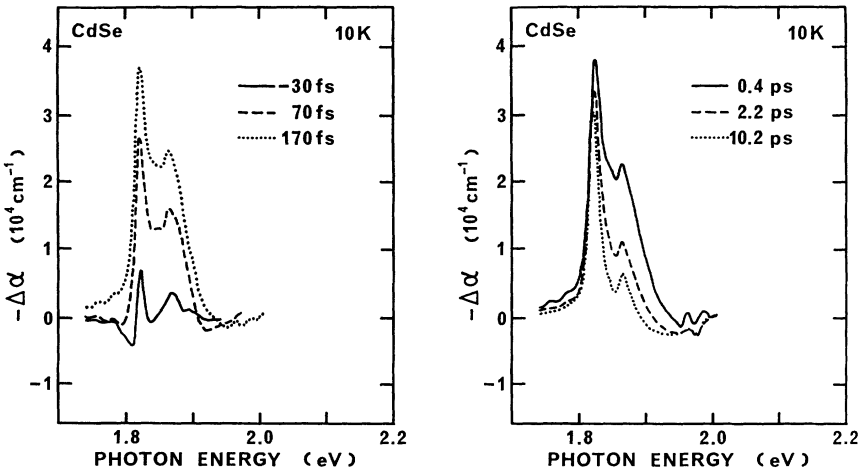

FIG. 11. Time-resolved absorption change $-\Delta\alpha$ observed under resonant excitation of the B exciton. The left-hand part shows spectra around the time origin and the right-hand part shows spectra in the picosecond regime.

the fast component and the slow component were found to be 0.9 and 53 ps, respectively.

Here, we discuss the fast recovery component. The recovery time of the B exciton's bleaching is much faster under B-exciton resonant excitation than under either A-exciton resonant excitation or band-to-band excitation. This is explained by a fast-scattering process from the B exciton to the A exciton.

The energy splitting between the A-hole band and the B-hole band, ΔE_{AB}, is 41 meV, as shown in Fig. 1.[23] Therefore, the photoexcited B exciton can emit a LO phonon and be transformed into an A exciton. The scattering time of the B exciton with the LO phonon, $1/\tau_{\rm LO}^{\rm ex}$, is estimated by using the Fröhlich interaction.[9,24] This process is the fastest among the exciton-phonon interactions. The scattering rate of the B exciton is obtained by integration of the square of the matrix element. As a result, $1/\tau_{\rm LO}^{\rm ex}$ is represented by

$$1/\tau_{\rm LO}^{\rm ex}=\frac{e^2\hbar\omega_{\rm LO}\mu_B}{4\pi\varepsilon_{\rm vac}\hbar^2}\left[\frac{1}{\varepsilon_\infty}-\frac{1}{\varepsilon_0}\right]\frac{N_{\rm LO}(T_L)+1}{\hbar k_A}\times\int\frac{(q_e-q_h)^2}{q}dq\ . \tag{4.2}$$

Here, $\hbar\omega_{\rm LO}$, μ_B, $\varepsilon_{\rm vac}$, ε_∞, ε_0, $N_{\rm LO}$, and k_A denote the LO-phonon energy, the reduced mass of the B exciton ($0.11m_0$), the dielectric constant of vacuum, the optical and static dielectric constants of CdSe, the LO-phonon occupation number, and the A-exciton wave vector, respectively. The range of integration is written by the inequality

$$k_A\left[1-\left[1-\frac{2\mu_A}{\hbar^2k_A^2}(\Delta E_{AB}-\hbar\omega_{\rm LO})\right]^{1/2}\right]<q<k_A\left[1+\left[1+\frac{2\mu_A}{\hbar^2k_A^2}(\Delta E_{AB}-\hbar\omega_{\rm LO})\right]^{1/2}\right]. \tag{4.3}$$

In Eq. (4.2), q_e and q_h denote the Fourier transform of the electron and hole charge-distribution functions that are represented by[24]

$$q_e=\left[1+\left[\frac{m_h}{m_e+m_h}\frac{qa_B}{2}\right]^2\right]^{-2},\qquad q_h=\left[1+\left[\frac{m_e}{m_e+m_h}\frac{qa_B}{2}\right]^2\right]^{-2}. \tag{4.4}$$

Inserting Eq. (4.4) into (4.2), we obtain a scattering time of 0.2 ps. The experimental value agrees with the calculated one within one order of magnitude. The disagreement between the experimental scattering time and the calculated scattering time may come from the hot-phonon effect of LO phonons.

Recently, a time-resolved reflection measurement was adopted to this study and a transition time of 0.9 ps was measured.[25] The time constant obtained by our experiment agrees with this value. However, in this reflection

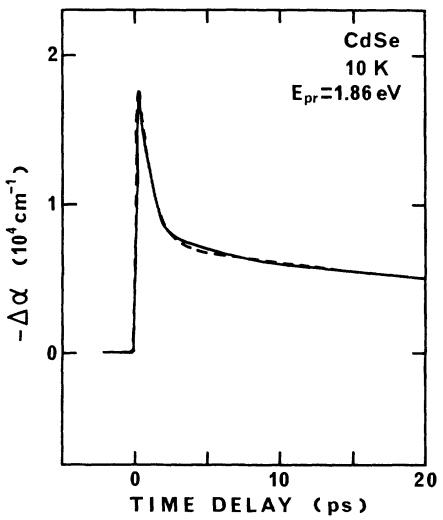

FIG. 12. The time dependence of bleaching observed at the B exciton. The solid line shows the experimental result. The dashed line shows the fit to a double-exponentially decaying function.

experiment, the time resolution (~0.6-ps pulse width) was comparable with the observed transition time. In our experiment, the time resolution was 110 fs, so that the recovery-time constant is measured with enough accuracy.

Another merit of this experiment is to observe the whole spectrum around the band edge, as shown in Fig. 11. As already mentioned, the B-exciton bleaching drastically decreases in the picosecond regime. We ascribed the fast recovery of this bleaching to the $B \rightarrow A$ transformation. Therefore, the population of the B exciton is expected to decrease. In contrast, the population of the A exciton is expected to increase. Both the populations modify the bleaching observed at the A exciton. From the experimental result, the bleaching observed at the A exciton decreases in the picosecond regime, as shown in the right-hand part of Fig. 11. The recovery of this bleaching is small but is found to have a fast component. The recovery-time constant observed at the A exciton is comparable with that observed at the B exciton. In our experimental condition, free carriers are also excited from the A-hole band. Therefore, the small recovery of the bleaching observed at the A exciton may come from the reduction of the free carriers or the B-exciton population.

V. CONCLUSIONS

In this work, ultrafast pump-and-white-continuum-probe spectroscopy was adopted to study the dynamical behavior of photogenerated carriers in a CdSe thin film. As a result, dynamics of photogenerated carriers in CdSe are clarified as follows.

Under band-to-band excitation, a nonthermalized hot-carrier distribution was observed during the pump pulse. The nonthermalized distribution was observed not only at the pump energy, but also on the low-energy side of the pump energy. This is due to the fast carrier-LO-phonon scattering process. The thermalization time could not be resolved in the experiment, but the ratio of the nonthermalized to the total carriers gave the thermalization time of 20–40 fs.

In the cooling process of photogenerated hot carriers, the carriers lose their excess energy by emitting phonons while maintaining a thermalized distribution. The observed slow carrier cooling rate is not explained by screening of the carrier-phonon interaction. This is probably explained by hot-phonon effects of both LO and TO phonons.

Under resonant excitation of the A exciton, broadening of the B exciton was observed. The observed broadening gave the A-exciton–B-exciton scattering time of 31 fs. This value is well explained by a rigid-sphere scattering model. This is an example of the interaction among different kinds of excitons.

Under resonant excitation of the B exciton, a fast recovery of the bleaching was observed at the B exciton. This fast recovery with a 0.9-ps time constant is well explained by transformation of the B exciton to the A exciton with emission of an LO phonon through the Fröhlich interaction.

ACKNOWLEDGMENTS

The authors are grateful to Professor H. Fujiyasu and Professor A. Ishida and their co-workers at Shizuoka University for the kind guidance regarding hot-wall epitaxy, and to S. Koide for the sample preparation. They also acknowledge Professor N. Peyghambarian, B. Fluegel, and K. Missner for critical reading of this manuscript. The measurements with resonant excitation of excitons were performed at the Optical Sciences Center, University of Arizona. This work was supported by the International Science Research Program No. 02044021 and the Scientific Research Grant-in-Aid No. 02952058 from the Ministry of Education, Science and Culture of Japan (MESC).

APPENDIX: ANISOTROPY OF THE BAND STRUCTURE

The absorption spectrum is proportional to the imaginary part of the susceptibility, expressed as[18]

$$\mathrm{Im}\chi(E) \propto \left[\frac{2\mu}{\hbar^2}\right]^{3/2} (E-E_g)^{1/2}\theta(E-E_g)N(E-E_g) \; . \tag{A1}$$

Here, E, μ, and E_g represent the photon energy, a reduced mass between an electron and a hole, and the energy gap, respectively. The step function $\theta(E-E_g)$ precludes absorption below the band gap. The phase space filling effect is taken into account in the term $N(E-E_g)$, which is represented by

$$N(E)=1-f(\alpha_e E-E_e^F)-f(\alpha_h E-E_h^F) \; . \tag{A2}$$

Here, E_e^F and E_h^F represent the electron and hole quasi-Fermi energies. The prefactors α_e and α_h mean μ/m_e and μ/m_h, respectively. The anisotropy in the band structure changes μ and $N(E-E_g)$. By using the aniso-

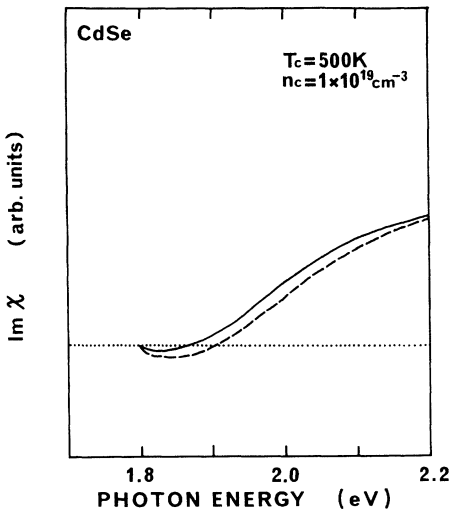

FIG. 13. The calculated imaginary part of the susceptibility. The solid line shows the anisotropic case and the dashed line shows the isotropic case.

tropic masses of the electron ($m_e^{\perp}$ and $m_e^{\parallel}$) and the hole ($m_h^{\perp}$ and $m_h^{\parallel}$), $N(E-E_g)$ is represented by[18]

$$N(E-E_g)=\int_0^1 ds\{1-f([\gamma+\eta s^2]E-E_e^F) -f([1-\gamma-\eta s^2]E-E_h^F)\}\ , \tag{A3}$$

$$\gamma=\frac{m_h^{\perp}}{m_e^{\perp}+m_h^{\perp}}\ ,\quad \eta=\frac{m_h^{\parallel}}{m_e^{\parallel}+m_h^{\parallel}}\ .$$

The effective masses of the electron and the hole are replaced by averaged values, $m_e=(m_e^{\perp 2}m_e^{\parallel})^{1/3}$ and $m_h=(m_h^{\perp 2}m_h^{\parallel})^{1/3}$. The anisotropic masses in CdSe were chosen as $m_e^{\perp}=m_e^{\parallel}=0.13m_0$, $m_h^{\perp}=0.45m_0$, and $m_h^{\parallel}=2.5m_0$, where m_0 denotes a bare electron mass.

Inserting Eq. (A3) into (A1), we obtained the imaginary part of the susceptibility, including the anisotropy of the hole band. Figure 13 shows the result obtained under a carrier temperature of 500 K and density of 1×10^{19} cm^{-3}. The band gap was fixed at 1.8 eV in both cases. The difference with and without the anisotropy is about 10% around 2.1 eV. Therefore, it is acceptable to neglect the anisotropy in the A-hole band.

[1]For a recent review, see J. Shah, IEEE J. Quantum Electron. **QE-22**, 1728 (1986); D. H. Auston, Phys. Today **43** (2), 46 (1990).

[2]J. L. Ouder, D. Hulin, A. Migus, A. Antonetti, and F. Alexandre, Phys. Rev. Lett. **55**, 2074 (1985).

[3]W. Z. Lin, R. W. Schoenlein, S. D. Brorson, J. G. Fujimoto, and E. P. Ippen, in *XV International Quantum Electronics Technical Digest Series* [Opt. Soc. Am. **21**, 82 (1987)]; C. H. Brito-Cruz, R. L. Fork, and C. V. Shank, *ibid.*

[4]W. H. Knox, C. Hirlimann, D. A. B. Miller, J. Shah, D. S. Chemla, and C. V. Shank, Phys. Rev. Lett. **56**, 1191 (1986).

[5]W. H. Knox, D. S. Chemla, G. Livescu, J. E. Cunningham, and J. E. Henry, Phys. Rev. Lett. **61**, 1290 (1988).

[6]N. Peyghambarian and S. W. Koch, Rev. Phys. Appl. **22**, 1711 (1987).

[7]P. C. Becker, H. L. Fragnito, C. H. Brito Cruz, R. L. Fork, J. E. Cunningham, J. E. Henry, and C. V. Shank, Phys. Rev. Lett. **61**, 1647 (1988); J.-Y. Bigot, M. T. Portella, R. W. Schoenlein, C. V. Shank, and J. E. Cunningham, in *Ultrafast Phenomena VII,* edited by C. B. Harris, E. P. Ippen, G. A. Mourou, and A. H. Zewail (Springer, Berlin, 1990), p. 239.

[8]M. J. Rosker, F. W. Wise, and C. L. Tang, Appl. Phys. Lett. **49**, 1726 (1986); W. Z. Lin, J. G. Fujimoto, E. P. Ippen, and R. A. Logan, *ibid.* **50**, 124 (1987); W. Z. Lin, J. G. Fujimoto, E. P. Ippen, and R. A. Logan, *ibid.* **51**, 161 (1987); P. C. Becker, H. L. Fragnito, C. H. Brito-Cruz, J. Shah, R. L. Fork, J. E. Cunningham, J. E. Henry, and C. V. Shank, *ibid.* **53**, 2089 (1988); W. Z. Lin, R. W. Schoenlein, J. G. Fujimoto, and E. P. Ippen, IEEE J. Quantum Electron. **QE-24**, 267 (1988).

[9]E. M. Conwell, in *Solid State Physics,* edited by F. Seitz, D. Turnbull, and H. Ehrenreich (Academic, New York, 1967), Suppl. 9.

[10]R. Ulbrich, Phys. Rev. B **8**, 5719 (1973).

[11]E. J. Yoffa, Phys. Rev. B **23**, 1909 (1981).

[12]S. M. Kogan, Fiz. Tverd. Tela (Leningrad) **4**, 2474 (1963) [Sov. Phys. Solid State **4**, 1813 (1963)].

[13]M. Pugnet, J. Collet, and A. Cornet, Solid State Commun. **38**, 531 (1981).

[14]J. Collet, A. Cornet, M. Pugnet, and T. Amand, Solid State Commun. **42**, 883 (1982); W. Potz and P. Kocevar, Phys. Rev. B **28**, 7040 (1982); P. Kocevar, Physica **134B**, 155 (1985); S. A. Lyon, J. Lumin. **35**, 121 (1986); K. Leo, W. W. Ruhle, and K. Ploog, Phys. Rev. B **38**, 1947 (1988).

[15]J. Shah, A. Pinczuk, A. C. Gossard, and W. Wiegmann, Phys. Rev. Lett. **54**, 2045 (1985).

[16]*Optical Nonlinearities and Instabilities in Semiconductors,* edited by H. Haug (Academic, New York, 1988).

[17]J. Shah, R. F. Leheny, and C. Lin, Solid State Commun. **18**, 1035 (1976); D. H. Auston, S. McAfee, C. V. Shank, E. P. Ippen, and O. Teschke, Solid-State Electron. **21**, 147 (1978).

[18]R. Zimmermann, *Many-Particle Theory of Highly Excited Semiconductors* (Teubner, Leipzig, 1988).

[19]Y. Masumoto and F. Sasaki, J. Lumin. **48/49**, 189 (1991).

[20]J. B. Stark, W. H. Knox, D. S. Chemla, W. Schäfer, S. Schmitt-Rink, and C. Stafford, Phys. Rev. Lett. **65**, 3033 (1990).

[21]L. Schultheis, J. Kuhl, A. Honold, and C. W. Tu, Phys. Rev. Lett. **57**, 1635 (1986); L. Schultheis, A. Honold, J. Kuhl, K. Kohler, and C. W. Tu, Phys. Rev. B **34**, 9027 (1986); A. Honold, L. Schultheis, J. Kuhl, and C. W. Tu, *ibid.* **40**, 6442 (1989).

[22]G. Manzke, K. Henneberger, and V. May, Phys. Status Solidi B **139**, 233 (1987).

[23]The energy splitting between the A exciton and B exciton in CdSe is usually about 25 meV. In our sample, energy shifts of both excitons were observed. We consider that the energy shifts are caused by strain between the mica substrate and the CdSe sample.

[24]C. Weisbuch and R. G. Ulbrich, in *Light Scattering in Solid III,* edited by M. Cardona and G. Güntherodt (Springer, Berlin, 1982), Chap. 7.

[25]D. Braun, W. W. Rühle, and J. Collet, in *Ultrafast Phenomena VII* (Ref. 7), p. 271.